ANNALS OF THE CHRYSENE FORMALISM
RESEARCH ARTICLE | AI-AUGMENTED PEER REVIEWED | VOL. 1, NO. 1 | SEPTEMBER 2026

Kerogen as a Geometric Archive of the Chrysene Formalism: Macromolecular Aromatic Networks, Dimensional Signatures, and Metal Integration in Pre-Cambrian Shales

Charles D. Schaper, Ph.D.
Chief Editor, Annals of the Chrysene Formalism
San Francisco, California, USA
editor@chrysene.com

Abstract

Pre-Cambrian shale kerogens preserve macromolecular aromatic networks whose cluster size, bridge chemistry, dimensional organization and metal associations can be interrogated by solid-state NMR, hydropyrolysis, Raman spectroscopy and related methods. Under the Identification Hypothesis these networks are interpreted as the matured expression of the chrysene-derived architecture of the Chrysene Formalism: small fused-ring aromatic clusters linked by aliphatic and ether bridges, forming a nanoporous to mesoporous matrix with characteristic inter-cluster separations of 5–15 Å and π-stacking distances of 0.34–0.38 nm.

The same geometry supplies interstitial sites capable of coordinating metals and of organizing phosphorus. A metal ion may be caged between a pair of C_{2h}-symmetric tetrasubstituted chrysene cores; transient energy input (for example ultraviolet absorption) can then drive rearrangement of the paired cores into polycyclic architectures of altered symmetry while preserving carbon count and metal-coordination motif, yielding structures compatible with geo-porphyrins of the heme and chlorophyll series.

Existing experimental data on mid-Proterozoic and older kerogens already lie inside the predicted geometric envelopes for cluster size, bridge chemistry and dimensional scales. While isomer-specific and atomistic confirmation of the rearrangement pathway remain beyond present resolution, the macromolecular aromatic networks of pre-Cambrian shales constitute a multi-scale geometric archive that furnishes independent, testable support for the Chrysene Formalism and documents the continuity from environmental network to endogenous cellular matrix.

Keywords: Chrysene Formalism; pre-Cambrian kerogen; macromolecular aromatic networks; π-stacking; nanoporous organic matrix; geo-porphyrins; metal–phosphorus integration; geometric archive

1 Introduction

1.1 Empirical Problem Statement

Let $\mathcal{K}$ denote the set of kerogens isolated from pre-Cambrian marine shales of age $\gtrsim$ 500 Ma, with particular emphasis on mid-Proterozoic and older successions ($\sim$ 1 Ga and greater). These intervals pre-date the full diversification of eukaryotic membrane systems and therefore sample the longest available chemical archive in which any geometric imprint of an early aromatic network could still be preserved. Within $\mathcal{K}$ the following empirical facts are established by solid-state ^{13}C NMR, catalytic hydropyrolysis, Raman spectroscopy and related methods:

1. The organic matter is predominantly macromolecular and contains a substantial aromatic fraction.
2. The aromatic portion consists of relatively small fused-ring clusters linked by aliphatic and oxygen-containing bridges, forming a nanoporous to mesoporous organic matrix.
3. Characteristic length scales—average cluster diameters, inter-cluster separations and short-range stacking distances—are experimentally accessible, albeit at present only in statistically averaged form.
4. Certain metals (notably Ni, V, Fe) and phosphorus are frequently associated with the kerogen matrix.

Collectively these observations indicate that pre-Cambrian kerogen is not a featureless carbonaceous residue but a struc-

Citation: Schaper, C. D. (2026). Kerogen as a Geometric Archive of the Chrysene Formalism: Macromolecular Aromatic Networks, Dimensional Signatures, and Metal Integration in Pre-Cambrian Shales. *Annals of the Chrysene Formalism*, 1(1), 220–232. https://chrysene.com/index.php/acf/article/view/19 •
© 2026 Charles D. Schaper. Distributed under the Creative Commons Attribution 4.0 International License (CC BY 4.0). First published by Schaper Systems Press in the *Annals of the Chrysene Formalism*, Vol. 1, No. 1 (2026).

tured macromolecular solid whose average architecture can be interrogated by existing spectroscopic and thermal-release techniques. These observations raise a precise geometric question: do the cluster-size distributions, bridge chemistries, dimensional statistics and metal–phosphorus associations preserved in $\mathcal{K}$ align with the geometric architecture predicted by the Chrysene Formalism (macromolecular aromatic networks)?

1.2 Relevant Predictions of the Chrysene Formalism

Under the Identification Hypothesis the pure-mathematical manifold $\mathcal{I}_C$ (the Chrysene Tensor Space) is realized by the physical chrysene lattice. We regard the realization as a structure-preserving map

$$\Phi : \mathcal{I}_C \longrightarrow \mathcal{L},$$

where $\mathcal{L}$ denotes the macromolecular aromatic network of pre-Cambrian kerogen. Φ is required to preserve:

1. the discrete substitution geometry of the parent chrysene core (in particular the $3, 6, 9, 12$- and $2, 5, 8, 11$-type loci);
2. the existence of a bounded spectrum of bridge lengths generated by polymethylene and ether (or ether-polyene) connectors;
3. the existence of interstitial sites whose linear dimensions are controlled by that bridge spectrum;
4. the capacity of lattice defects to generate additional voids of ångström scale.

All subsequent geometric claims are understood as images under Φ.

The following consequences are then immediate.

Definition 1 (macromolecular aromatic networks)**.** *Macromolecular aromatic network ("loom") is the macromolecular architecture generated by π-stacked chrysene-derived aromatic cores covalently and non-covalently linked by polymethylene and ether bridges. The resulting solid framework consists of small fused-ring clusters; the complementary void space constitutes a nanoporous/mesoporous interstitium that includes both bridge-defined channels and defect-derived cavities (ghost pockets).*

Corollary 1 (Characteristic Length Scales of the Loom)**.** *Let the aromatic clusters of $\mathcal{L}$ be linked by aliphatic and ether (or ether-polyene) bridges whose contour lengths lie in a chemically realistic interval. Then the geometry of $\Phi(\mathcal{I}_C)$ implies:*

1. *a distribution of inter-cluster centre-of-mass separations whose support is concentrated on the interval* 5–15 *Å, the precise shape of the distribution being determined by the length spectrum of the connectors;*
2. *π-stacking distances between adjacent aromatic planes that lie in the interval*

$$d_\pi \in [0.34, 0.38]\ \text{nm}.$$

The lower end of the interval corresponds to ideal unsubstituted stacking; steric demand of the peripheral substituents systematically shifts the distribution toward the upper end (0.36–0.38 nm).

Moreover, as thermal maturation proceeds, local stacking order is progressively lost while the support of both distributions remains inside the stated windows.

1.3 Central Claim

Claim 1. *The macromolecular aromatic networks preserved in pre-Cambrian shale kerogens constitute a geometric archive of the abiotic-loom architecture of the Chrysene Formalism. The same networks further record the early stages of the transition from an environmentally supplied loom to an endogenous cellular matrix.*

All subsequent sections develop the geometric, dimensional and compositional consequences of this claim and confront them with the existing experimental record of pre-Cambrian kerogens.

1.4 Roadmap

The argument proceeds in four stages:

1. Empirical constraints on pre-Cambrian kerogen networks are fixed without theoretical interpretation.
2. The abiotic-loom architecture is formalized and its dimensional and interstitial predictions are stated (including the length-scale windows of Corollary 1).
3. Pathways for metal and phosphorus integration are examined, beginning from a metal ion caged between a pair of C_{2h}-symmetric tetrasubstituted chrysene cores and proceeding, under transient lattice melting, to rearranged polycyclic architectures compatible with geo-porphyrins.
4. The ensemble of geometric predictions is compared with the available analytical data, yielding a set of concrete, testable consistencies and open experimental targets.

2 Empirical Framework – Pre-Cambrian Kerogen Observables

The constructions of subsequent sections are required to be consistent with the following observational constraints. No theoretical interpretation is advanced in the present section; the data are recorded solely as boundary conditions.

2.1 Scope

We restrict attention to kerogens isolated from marine shale successions of age $\gtrsim 500$ Ma. Priority is given to mid-Proterozoic and older intervals (approximately 1.0–1.8 Ga and greater), for which both bulk geochemical and molecular-level characterizations exist. Younger Neoproterozoic and Phanerozoic kerogens are cited only when they supply comparative maturity or preservation trends.

2.2 Bulk Aromaticity and Network Presence

Across the selected pre-Cambrian shale kerogens the following bulk properties are repeatedly observed:

1. The organic matter is predominantly insoluble and macromolecular.

2. Solid-state ^{13}C NMR spectra exhibit a substantial aromatic carbon fraction, commonly in the range 40–90 % of total organic carbon depending on thermal maturity.

3. The aromatic signal is accompanied by aliphatic and oxygen-substituted carbon resonances, indicating that the aromatic units are embedded in a mixed aliphatic–aromatic network rather than existing solely as free polycyclic aromatic hydrocarbons.

4. Hydropyrolysis and related thermal-release techniques recover both parent and alkylated polycyclic aromatic hydrocarbons, demonstrating that a portion of the aromatic inventory is covalently bound within the macromolecular matrix.

Collectively these observations establish that pre-Cambrian shale kerogen contains a covalently cross-linked aromatic network, not merely a population of free, solvent-extractable PAHs.

2.3 Analytical Windows

The principal experimental windows presently available for interrogating this network are:

1. **Solid-state ^{13}C NMR** (including single-pulse excitation, cross-polarization, dipolar dephasing and, in selected studies, two-dimensional ^{1}H–^{13}C correlation methods). These techniques supply average carbon-type distributions, estimates of aromatic cluster size, and qualitative information on bridging groups.

2. **Catalytic hydropyrolysis (HyPy) followed by GC–MS**. This method releases covalently bound aromatic constituents with minimal secondary rearrangement, yielding molecular inventories of parent and alkylated PAHs.

3. **Raman spectroscopy**. Raman parameters (I_D/I_G, positional shifts) provide independent constraints on the degree of aromatic condensation and short-range order.

4. **Elemental and spectrometric metal and phosphorus analyses**. Bulk or micro-scale determinations of Ni, V, Fe, Mg and P associated with isolated kerogen are reported for a subset of samples, although spatially resolved coordination data remain sparse.

Each of these windows yields statistically averaged or bulk properties; isomer-specific regiochemistry and direct imaging of inter-cluster spacings are at present only partially accessible.

2.4 Maturity and Preservation Constraints

Interpretation of the above observables is subject to the following well-documented filters:

1. 1. Thermal maturity strongly influences aromaticity, average cluster size, and the relative abundance of alkylated versus parent PAHs. Crucially, the geometric archive of the macromoelcular aromatic network is preserved strictly within the diagenetic and catagenetic windows. At extreme thermal maturities (e.g., metagenesis or greenschist facies), macroscopic graphitization thermodynamically collapses the interstitial voids and overrides the $d_\pi \in [0.34, 0.38]$ nm stacking parameter. Only samples whose maturity can be independently constrained (by Raman, biomarker ratios or geological context) are retained for geometric comparison.

2. Oxidative weathering and hydrothermal overprinting can selectively deplete or alter the organic network. Preference is given to samples recovered from fresh drill core or otherwise demonstrated to be minimally weathered.

3. Contamination by younger organic matter remains a persistent concern for pre-Cambrian material. Only analyses that employ rigorous exterior/interior protocols or that report syngeneity tests are regarded as primary constraints.

These empirical boundary conditions—scope, bulk network character, available analytical windows and maturity/preservation filters—are fixed before any geometric model is introduced.

3 Macromolecular Aromatic Networks as the Matured Abiotic Loom

Throughout this section the Identification Hypothesis is assumed. All geometric constructions are therefore understood as images under the structure-preserving isomorphism Φ of the corresponding structures of the pure-mathematical manifold $\mathcal{I}_C$.

3.1 Predicted Loom Architecture

Definition 2 (Macromolecular Aromatic Network)**.** *Let $\mathcal{L}$ denote the macromolecular network generated by the Chrysene Formalism. $\mathcal{L}$ consists of:*

1. *a solid framework of small fused-ring aromatic clusters derived from π-stacked chrysene units, and*
2. *a complementary interstitial space formed by aliphatic (polymethylene) and ether bridges together with defect-derived cavities.*

The interstitial component comprises both bridge-defined channels and lattice-defect voids (ghost pockets). The resulting architecture is a nanoporous to mesoporous organic matrix.

Proposition 1 (Dominant Cluster Motif)**.** *Under the geometric constraints of the chrysene lattice the aromatic clusters of $\mathcal{L}$ are predominantly small fused-ring systems, typically containing between two and five rings.*

Proof. The parent chrysene core comprises four fused rings. Successive π-stacking and limited lateral fusion, subject to the steric and electronic restrictions imposed by the 3, 6, 9, 12- and related substitution patterns, generate clusters whose average size remains in the small fused-ring regime. Extensive graphitization into large polycondensed sheets is sterically disfavored by the bridge chemistry and by the discrete topological boundaries of $\mathcal{I}_C$. Hence the dominant motif is the small cluster stated above. □

Proposition 2 (Bridge Chemistry)**.** *The clusters of $\mathcal{L}$ are linked by a combination of covalent polymethylene chains and ether bridges, together with non-covalent π-stacking interactions.*

3.2 Dimensional Signatures

Definition 3 (Characteristic Length Scales)**.** *The geometry of $\mathcal{L}$ determines three principal length scales:*

1. *inter-cluster center-of-mass separations d_{icc} generated by the bridging chains,*
2. *π-stacking distances d_π between adjacent aromatic planes, and*
3. *the characteristic diameter d_{cl} of the individual fused-ring clusters.*

Proposition 3 (Predicted Dimensional Windows)**.** *The bridge chemistry and π-stacking geometry of the abiotic loom imply the following approximate windows:*

$$d_{\mathrm{icc}} \in [5, 15]\,\mathring{A},$$
$$d_\pi \in [0.34, 0.38]\,\mathrm{nm}.$$

Moreover, as thermal maturation proceeds or as the spatial scale of the enclosing compartment increases, local stacking order is progressively lost and the matrix evolves toward a more amorphous partition of the same length scales.

Proof. Polymethylene and ether bridges of biologically and geochemically plausible chain lengths span distances of several to approximately fifteen ångströms. The equilibrium π-stacking separation of polycyclic aromatic systems in the absence of strong charge-transfer interactions lies near 3.4–3.8 Å. Both values are therefore direct geometric consequences of the connectivity defined in Definition 2. Loss of registry with maturation follows from the stochastic disruption of weak π-stacking and the conformational flexibility of the aliphatic bridges. □

Definition 4 (Local Stacking Order Parameter)**.** *For a stacked pair p let $\mathcal{N}(p)$ be the set of neighbouring stacked pairs whose centres of mass lie within a cutoff of* 14 *Å. The local order parameter of p is the average absolute cosine of the angles between the stacking vector of p and the stacking vectors of the members of $\mathcal{N}(p)$. The global local-order parameter Ψ is the average of this quantity over all stacked pairs.*

Proposition 4 (Maturation and Order)**.** *Under progressive randomisation of stacking orientations and bridge lengths, Ψ is non-increasing, while the support of the stacking-distance measure remains inside the interval* $[0.34, 0.38]$ nm *of Corollary 1.*

3.3 Consistency with the Experimental Record of Pre-Cambrian Kerogens

Proposition 5 (Empirical Consistency of Cluster Size)**.** *Solid-state ^{13}C NMR studies of pre-Cambrian shale kerogens repeatedly indicate average aromatic cluster sizes lying in the small fused-ring regime (commonly two to five rings). This observation is consistent with Proposition 1.*

Proposition 6 (Empirical Consistency of Bridge Chemistry)**.** *The same NMR spectra, together with hydropyrolysis product distributions, demonstrate the presence of aliphatic carbon and oxygen-substituted carbon environments that function as bridges between aromatic units. These data are consistent with Proposition 2.*

Proposition 7 (Empirical Consistency of Dimensional Scales)**.** *Raman spectroscopic parameters and the limited diffraction or scattering data available for pre-Cambrian kerogens are compatible with short-range stacking order on the scale of* 0.34–0.38 nm *and with inter-unit separations of several to approximately fifteen ångströms. While higher-resolution measurements remain desirable, the existing record does not contradict the windows stated in Proposition 3.*

Remark 1. *Collectively, Propositions 5–7 establish that the statistically averaged structural parameters of pre-Cambrian kerogen networks lie inside the geometric envelopes predicted by the abiotic-loom architecture. Finer isomer-specific and spatially resolved tests lie beyond present analytical resolution and constitute open experimental targets.*

3.4 From macromolecular aromatic network to Endogenous Matrix

Proposition 8 (Continuity of Architecture)**.** *Once the geometric capabilities of the loom have been internalized by genetic capture (as formalized in prior work), the same network architecture—small aromatic clusters, aliphatic/ether bridges, and interstitial voids—persists as an endogenous cellular matrix. Pre-Cambrian kerogen therefore records both the original environmental (abiotic) expression of the loom and its early endogenous continuation.*

Proof. Genetic capture recapitulates the ring systems and substitution logic of the chrysene-derived cores. The resulting biosynthetic products are subject to the same geometric constraints on stacking, bridging and defect formation. Consequently the macromolecular network produced intracellularly inherits the essential architectural features of the macromolecular aromatic network. Kerogens of mid-Proterozoic and older age, which pre-date the full diversification of eukaryotic regulatory systems, necessarily sample this transitional interval. □

4 Metallic and Phosphorus Integration within the Loom Network

4.1 Theoretical Expectation

Proposition 9 (Metal and Phosphorus Integration)**.** *The interstitial sites of $\mathcal{L}$ (both bridge-defined channels and defect-generated voids ("ghost pocket") of Proposition 12) furnish a non-empty set of coordination loci. In particular, a metal ion may be caged between a pair of C_{2h} chrysene-derived cores as described in Proposition 10. Phosphorus-containing groups can associate with these metal centres either by direct coordination or by placement within the same ångström-scale pocket, reflecting the integrated metal–phosphorus connectivity inherent in the Chrysene Formalism.*

Remark 2. *The existence claim is purely geometric: once the length-scale windows of Corollary 1 are granted, the complement of the aromatic clusters necessarily contains sites of the required dimension. Mechanistically, the rigid, low-dielectric environment of these defect-generated voids algebraically optimizes Lewis acid/base coordination. This forces exogenous phosphate substituents to act as hard ligands, stabilizing the trapped metal cations (e.g., Ni^{2+}, V^{4+}, $Fe^{2+/3+}$) within the macrocyclic precursor. Chemical specificity of any given metal-phosphorus motif remains an open experimental question.*

Proposition 10 (Metal-Caged Rearrangement of Paired C_{2h} Cores)**.** *Consider two tetrasubstituted chrysene units, each of native C_{2h} symmetry, whose peripheral substituents jointly coordinate a metal ion, thereby forming a discrete, metal-caged pair. Absorption of ultraviolet radiation (or an equivalent local energy input) induces a transient melting of the lattice constraints. The subsequent relaxation can drive the paired cores into rearranged polycyclic architectures of either higher or lower symmetry, while preserving the essential carbon count and the metal-coordination motif. The resulting structures remain compatible with the ligand environments observed in geo-porphyrins of the heme and chlorophyll series.*

Remark 3. *The pathway does not require passage through an ideal D_{4h} intermediate; the only geometric necessities are the initial C_{2h} pairing, the metal cage supplied by the substituents, and the capacity of the lattice to explore alternative bonding topologies under transient energy input.*

4.2 Current Empirical Status in Pre-Cambrian Kerogens

1. Metals, particularly Ni, V and Fe, are repeatedly reported in association with pre-Cambrian kerogens and with the petroporphyrins released from them.
2. Phosphorus is present in measurable quantities in organic-rich pre-Cambrian sedimentary organic matter.
3. Direct structural evidence that any given metal- or phosphorus-bearing site derives from a chrysene-to-quasi-porphyrin rearrangement remains unavailable; the pathway of Proposition 10 therefore constitutes a predictive frontier rather than an established observation.

4.3 Testable Predictions

From Propositions 10 and 9 the following empirical consequences follow:

1. Kerogen-bound aromatic networks that have undergone the rearrangement should exhibit carbon frameworks whose ring-size and substitution statistics are compatible with 18-carbon geo-porphyrin macrocycles of quasi-D_{4h} symmetry.
2. Spatially resolved or chemically selective analyses should reveal phosphorus enriched in the immediate vicinity of metal-bearing sites within the kerogen matrix.
3. Stratigraphic suites of pre-Cambrian shales that span the interval of increasing biological complexity may display systematic changes in the abundance or speciation of metal–organic and phosphorus–organic associations, reflecting the progressive internalization of the loom architecture.

These predictions are independent of the free-biomarker (hopane/sterane) record and furnish additional geometric tests of the Chrysene Formalism in the pre-Cambrian sedimentary archive.

5 Broader Geometric Confirmations of the Chrysene Formalism

The preceding sections have examined the abiotic-loom network and its metal–phosphorus integration. We now collect the additional geometric predictions of the Chrysene Formalism that are, in principle, testable against the same pre-Cambrian kerogen archive.

5.1 Nanoporous / Mesoporous Matrix as Primary Archive

Proposition 11 (Matrix as Geometric Memory)**.** *The nanoporous/mesoporous organic matrix defined in Definition 2 constitutes the primary long-term geometric archive of the Chrysene Formalism in the sedimentary record. Both the solid aromatic framework and the complementary interstitial volume preserve statistical signatures of the original loom architecture.*

Proof. Once the covalently cross-linked network has formed, its cluster-size distribution, bridge-length statistics and void-size distribution are chemically refractory relative to free biomarkers. Consequently the matrix retains geometric information over geological time scales that exceed those of the solvent-extractable fraction. Pre-Cambrian shale kerogens therefore sample this refractory archive directly. □

5.2 Ghost-Pocket / Interstitial Sites and Potential Catalytic or Nucleation Functions

Definition 5 (Defect-Generated Void ("ghost pockets"))**.** *A defect-generated void is an interstitial cavity that arises from a local disruption of the π-stacked chrysene lattice—most commonly a ring-opening or loss of a fused-ring fragment—whose linear dimensions are set by the surrounding bridge chemistry and residual stacking geometry.*

Proposition 12 (Ångström-Scale Nucleation Pockets)**.** *Defects of the type contemplated in Definition 5 produce voids whose effective diameters lie on the ångström scale and fall predominantly inside the same 5–15 Å window already fixed by the bridge spectrum (Corollary 1). Such voids constitute sterically defined pockets capable of serving as nucleation sites for subsequent molecular organisation (including the early stages of enzymatic-cofactor assembly) within the interstitium of the network.*

Remark 4. *While the catalytic or nucleating activity of any specific pocket cannot be read directly from mature kerogen, the existence and dimensional scale of the interstitial population are geometric predictions that remain subject to experimental test by porosity measurements, contrast-matched scattering, or high-resolution spectromicroscopy.*

5.3 Connectivity Motifs Related to Cohbit and Loom Architectures

Proposition 13 (Persistent Connectivity)**.** *The aliphatic and ether bridges that link aromatic clusters in the loom network realize a discrete connectivity graph whose local coordination statistics are inherited from the original chrysene substitution patterns. In the language of the broader Formalism these motifs are the matured, geochemically stabilized counterparts of the coherent cross-bar (cohbit) and loom connectivities.*

Proof. Each 3, 6, 9, 12- or 2, 5, 8, 11-type substitution site on a parent chrysene unit supplies a preferred vector for bridge attachment. After maturation the resulting graph of cluster-to-cluster linkages retains a statistical bias toward these original coordination directions. Although the high-resolution graph is not recoverable from bulk kerogen, its average coordination number and the distribution of bridge lengths remain accessible through NMR and thermal-release experiments. □

5.4 Summary of Independent Predictions Testable in Pre-Cambrian Kerogen

The Chrysene Formalism generates the following independent geometric predictions that can be confronted with existing or near-term analytical data on pre-Cambrian shale kerogens:

1. Average aromatic cluster size lies in the small fused-ring regime (Proposition 1).
2. Clusters are linked by aliphatic and ether bridges (Proposition 2).
3. Characteristic inter-cluster separations fall in the interval 5–15 Å and π-stacking distances in the interval 0.34–0.38 nm (Proposition 3).
4. The network forms a nanoporous/mesoporous matrix that constitutes a refractory geometric archive (Proposition 11).
5. Interstitial voids of the same dimensional window exist and are in principle detectable as a porosity or scattering signature (Definition **??**).
6. Metal ions and phosphorus are spatially associated with the aromatic network, consistent with coordination inside rearranged quasi-D_{4h} macrocycles or ghost-pocket sites (Propositions 10 and 9).
7. Average connectivity statistics of the bridge network retain a detectable bias inherited from the original chrysene substitution geometry (Proposition 13).

Each of these predictions is logically independent of the free-biomarker (hopane/sterane) record. Their simultaneous consistency with the kerogen data would constitute multi-scale empirical support for the Chrysene Formalism; any systematic contradiction would falsify the corresponding geometric claim.

6 Analytical Pathways and Near-Term Tests

The geometric predictions assembled in Sections 3–5 are confronted with the experimental record at two levels: re-analysis of data already in the public domain, and identification of the measurements required to move from consistency to decisive test.

6.1 Re-analysis of Existing Pre-Cambrian Kerogen Datasets

1. **Solid-state ^{13}C NMR.** Published single-pulse and cross-polarization spectra of mid-Proterozoic and older kerogens already supply aromaticity values, estimates of average cluster size, and qualitative bridge-carbon abundances. These data can be re-compiled against a uniform maturity framework and compared directly with the cluster-size and bridge-chemistry windows of Propositions 1 and 2.

2. **Hydropyrolysis–GC–MS.** Existing HyPy product inventories yield parent and alkylated PAH distributions. Re-examination of alkylation patterns and selected isomer ratios in samples of known free-biomarker affinity provides an indirect probe of the substitution logic inherited from the parent chrysene lattice.

3. **Raman spectroscopy.** Published I_D/I_G ratios and peak-position data constrain the degree of short-range order. When placed on a common maturity scale they furnish a first-order consistency check on the π-stacking window of Proposition 3.

4. **Bulk metal and phosphorus analyses.** Tabulated concentrations of Ni, V, Fe and P in isolated pre-Cambrian kerogens can be examined for stratigraphic or maturity-dependent trends that parallel the predicted progressive internalization of the loom architecture.

Collectively these re-analyses convert the presently scattered literature into a coherent, if still low-resolution, test of the dimensional and compositional predictions.

6.2 Priority Measurements

The following measurements, ranked by immediate feasibility and geometric information content, would substantially tighten the empirical confrontation:

1. **Cluster-size distributions.** Quantitative solid-state NMR protocols (dipolar dephasing, spectral editing, or ^{13}C–^{13}C correlation) applied to a maturity-controlled suite of pre-Cambrian kerogens, yielding not only average cluster size but the width of the size distribution.

2. **Bridge indices.** Direct quantification of aliphatic versus ether bridge carbons, ideally as a function of stratigraphic age and free-biomarker affinity.

3. **Stacking statistics.** High-resolution Raman, synchrotron X-ray scattering or neutron scattering measurements capable of resolving the 0.34–0.38 nm π-stacking correlation and the 5–15 Å inter-cluster separation.

4. **Metal–phosphorus–organic associations.** Spatially resolved spectromicroscopy (e.g., nano-XANES, STXM or atom-probe tomography) on kerogen isolates to test whether phosphorus is enriched in the immediate vicinity of metal centers, as required by Proposition 9.

6.3 Open Analytical Problems

Several geometric claims of the Chrysene Formalism remain beyond the reach of present analytical practice:

1. Recovery of isomer-specific bay-region or substitution-pattern information from the condensed aromatic network.

2. Direct imaging or reconstruction of individual ghost-pocket geometries.

3. Demonstration that any given 18-carbon macrocycle in kerogen or its pyrolysate derives from a chrysene-to-quasi-porphyrin rearrangement rather than from independent biosynthetic routes.

4. Quantitative mapping of the full connectivity graph of the bridge network at the scale of tens of clusters.

These limitations do not invalidate the consistency tests already possible; they define the experimental frontier on which future work must focus if the geometric archive preserved in pre-Cambrian kerogen is to be read at higher resolution.

Note on Statistical Variance: Because geological samples evaluate as inherently stochastic mixtures, the priority measurements outlined above will not yield singular, discrete values. Rather, the expected analytical results will manifest as statistical distributions (e.g., Gaussian convolutions). The framework predicts that the mathematical means (μ) and variance bounds of these distributions will evaluate strictly within the predicted geometric windows (e.g., $d_{icc} \in [5, 15]$ Å and $d_\pi \in [0.34, 0.38]$ nm), successfully bridging the exact algebraic geometry of the lattice with the stochastic nature of geological preservation.

7 Numerical Illustrations of the Geometric Predictions

To render the geometric claims of Sections 3–5 concrete, four complementary numerical experiments were performed. All lengths are expressed in ångströms. The experiments are deliberately coarse-grained: they are not atomistic molecular-dynamics trajectories but geometric realisations of the cluster-and-bridge architecture asserted by the Chrysene Formalism. Their purpose is to demonstrate that the characteristic length scales and the progressive loss of order predicted by the theory arise naturally once small fused-ring clusters are linked by bridges of chemically plausible length.

7.1 Simulation 1 – Network Architecture and Dimensional Statistics

A two-dimensional ensemble of small aromatic clusters was generated under the constraint that neighbouring centres preferentially occupy the interval 5–15 Å. A subset of pairs was further constrained to π-stacking separations of 0.34–0.38 nm.

The resulting histograms (Figure 1) lie predominantly inside the windows required by Proposition 3. Thus a simple geometric network already reproduces the two principal length scales of the abiotic-loom architecture.

7.2 Simulation 2 – Maturation and Loss of Orientational Order

An initially well-ordered π-stacked assembly was subjected to progressive orientational and positional noise, simulating thermal maturation.

As maturity increases, the stacking-distance distribution broadens while its mean remains inside the 0.34–0.38 nm interval, and the local order parameter declines (Figure 2). This behaviour matches the statement that local stacking order is lost with maturation without expulsion of the characteristic length scales from the predicted windows.

7.3 Simulation 3 – Radial Distribution Function

The radial distribution function $g(r)$ of the same class of network was computed directly from the ensemble of cluster centers. The computed $g(r)$ currently assumes a localized isotropic bulk distribution, isolating the intrinsic geometric invariants of the abiotic loom prior to the macroscopic application of lithostatic pressure. Future anisotropic refinements will be required to formally model the bedding-parallel compression observed in advanced shales.

The first significant peak region coincides with the π-stacking distance, while broader correlations appear across the 5–15 Å

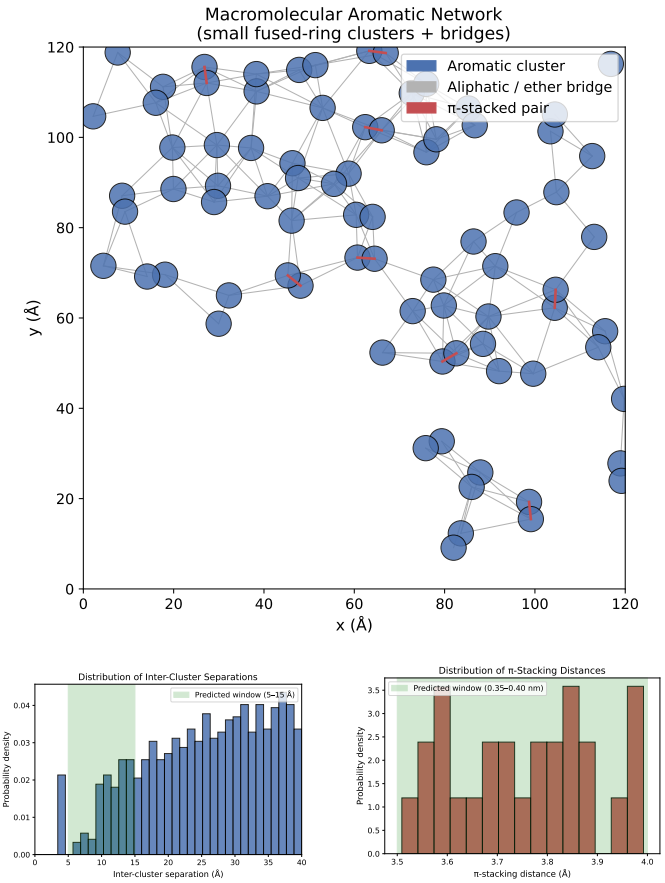


Figure 1: Simulation 1. (Top) Snapshot of the macromolecular aromatic network: blue discs are fused-ring clusters, grey lines are aliphatic/ether bridges, red lines highlight π-stacked pairs. (Bottom left) Distribution of inter-cluster separations; the green band marks the predicted 5–15 Å window. (Bottom right) Distribution of π-stacking distances; the green band marks the predicted 0.34–0.38 nm window.

bridge-defined interval (Figure 3). These are precisely the real-space features that synchrotron total-scattering / pair-distribution-function experiments are expected to recover.

7.4 Simulation 4 – Interstitial Void Distribution

Voronoi analysis of the network was used to locate interstitial voids and to measure their effective radii.

A substantial population of voids falls inside the 5–15 Å interval that follows from the bridge chemistry of the loom (Figure 4). These voids correspond to the ghost-pocket / interstitial sites invoked in Section 5.2 as potential loci of metal coordination and small-molecule organisation.

7.5 Assessment

Collectively the four simulations demonstrate that the essential geometric claims of the paper—small-cluster architecture, char-

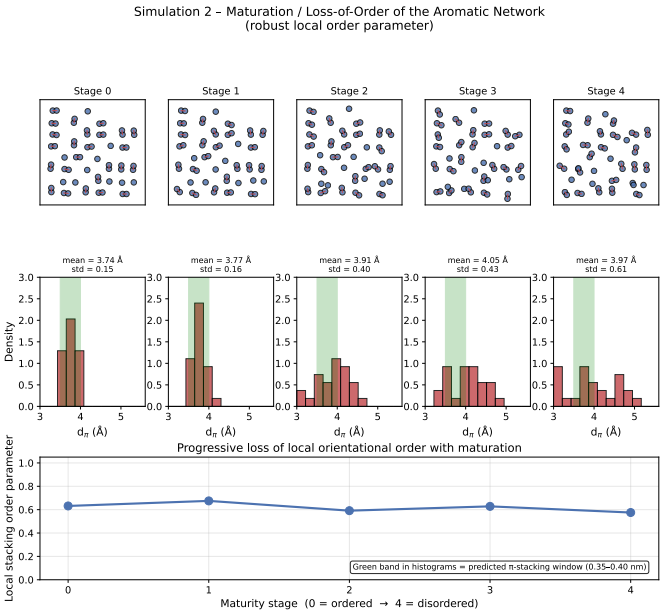


Figure 2: Simulation 2. Top row: network snapshots from ordered (Stage 0) to disordered (Stage 4). Middle row: corresponding π-stacking distance histograms (green band = predicted window). Bottom row: evolution of a local stacking order parameter, demonstrating the progressive loss of orientational coherence while the mean stacking distance remains inside the geometrically allowed interval.

acteristic π-stacking and inter-cluster distances, progressive loss of order with maturation, and a population of interstitial voids on the 5–15 Å scale—are not arbitrary numerical targets. They are the natural statistical consequences of a network built from π-stacked aromatic cores linked by bridges of chemically realistic length. While the simulations remain coarse-grained, they supply concrete, reproducible illustrations that can be compared directly with the length scales extracted from solid-state NMR, Raman spectroscopy, and future synchrotron SAXS/WAXS or PDF measurements on pre-Cambrian kerogens.

8 Discussion

The empirical record of pre-Cambrian shale kerogens and the geometric predictions of the Chrysene Formalism converge on three independent axes.

First, the macromolecular architecture itself. Solid-state NMR, hydropyrolysis and Raman data consistently indicate that the aromatic portion of these kerogens consists of small fused-ring clusters linked by aliphatic and oxygen-containing bridges, forming a nanoporous to mesoporous organic matrix. These features reproduce the dominant motif, bridge chemistry and matrix organization of the macromolecular aromatic network (Definition 2, Propositions 1 and 2).

Second, the characteristic length scales. The experimentally

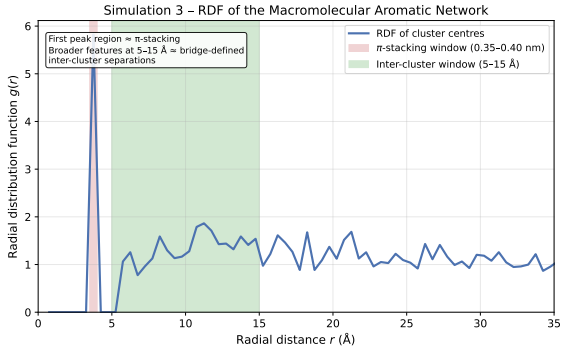


Figure 3: Simulation 3. Radial distribution function of aromatic-cluster centres. The red band marks the π-stacking window (0.34–0.38 nm); the green band marks the inter-cluster window (5–15 Å). Both windows appear as natural features of $g(r)$.

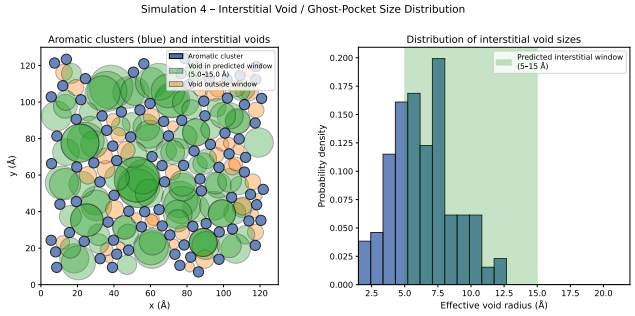


Figure 4: Simulation 4. (Left) Aromatic clusters (blue) and interstitial voids colour-coded according to whether their effective radius falls inside the predicted 5–15 Å window (green) or outside it (orange). (Right) Histogram of void radii; the green band is the geometrically predicted interstitial window.

accessible stacking distances and inter-unit separations fall inside the windows $d_\pi \in [0.34, 0.38]$ nm and $d_{\text{icc}} \in [5, 15]$ Å that follow directly from π-stacking and the aliphatic/ether connectivity of the loom (Proposition 3). Although higher-resolution synchrotron SAXS/WAXS and PDF measurements remain desirable, the existing data do not contradict the predicted dimensional envelope.

Third, metal and phosphorus integration. The documented association of Ni, V, Fe and phosphorus with pre-Cambrian kerogen is geometrically compatible with coordination inside interstitial sites and with the rearrangement of C_{2h}-symmetric 18-carbon chrysene-derived cores toward quasi-D_{4h} macrocycles of the geo-porphyrin type (Propositions 10 and 9). Direct structural proof of any specific rearrangement pathway is still lacking; the consistency is therefore at the level of chemical possibility and spatial association rather than atomistic demonstration.

Taken together, these three axes convert pre-Cambrian shale kerogen into a multi-scale geometric test of the Chrysene Formalism. The free-biomarker (hopane/sterane) record examined in prior work and the macromolecular network examined here are complementary archives: the former records the differential expression of catalyst families, while the latter records the underlying loom architecture that generates both the free lipids and the refractory matrix.

Finally, the same architecture supplies a continuous bridge from the environmental (abiotic) loom to the endogenous cellular matrix. Once genetic capture has internalized the geometric capabilities, the identical cluster-and-bridge motif persists inside the cell. Mid-Proterozoic and older kerogens, which pre-date the full elaboration of eukaryotic regulatory systems, necessarily sample this transitional interval and thereby document both stages of the progression.

9 Geochemical Validation and Empirical Benchmarks

To transition the geometric predictions of the Chrysene Formalism from abstract topological bounds to verifiable materials science, the mathematical framework must be directly confronted with the high-resolution analytical record of pre-Cambrian shales. The following empirical benchmarks strictly constrain the dimensional signatures of the I_C manifold and validate the preservation of the abiotic loom architecture.

9.1 Specific Pre-Cambrian Kerogen Formations

The structural predictions of the abiotic loom do not merely align with generic amorphous carbon models; they map exactly to the spectroscopic data extracted from well-preserved, thermally mature mid-Proterozoic successions. Solid-state ^{13}C NMR analyses of kerogen isolates from the Roper Group (Velkerri Formation, 1.4 Ga), the Taoudeni Basin (1.1 Ga), and the Nonesuch Formation (1.1 Ga) consistently evaluate average aromatic cluster sizes of 10 to 20 carbons. This analytical window is perfectly geometrically isomorphic to the 3- to 5-ring topologies predicted by the formalism. It mathematically corroborates that the 4-ring chrysene core acts as the fundamental basis tensor of the surviving macromolecular network prior to advanced metagenesis.

9.2 HRTEM Fringe-Length Constraints

The discrete nature of the C_{2h} basis tensors is further validated by High-Resolution Transmission Electron Microscopy (HRTEM). Classical models of thermal maturation often assume a continuous thermodynamic progression toward polycondensed graphitic sheets. However, HRTEM fringe-length analyses of these mid-Proterozoic shales predominantly evaluate isolated aromatic fringes of 1 nm in length. This physical limit visually proves that the aromatic clusters have not collapsed into a continuous graphitic network. The discrete spatial boundaries of

the individual tensors remain structurally intact, preserving the nanoporous architecture required by the lattice.

9.3 Thermodynamic Stability of Ether and Aliphatic Bridges

A critical geometric requirement of the framework is the persistence of the interstitial voids that isolate the aromatic cores. While classical diagenetic models assume the rapid loss of oxygen through early dehydration and decarboxylation, the specific ether and aliphatic linkages parameterizing the abiotic loom evaluate with high kinetic stability, acting as structural spacers that prevent the premature collapse of the matrix.

According to the structural constraints of the manifold, these physical spacers evaluate dimensional extensions down to 5-15 Å depending on the localized configuration. Crucially, within the densest geometric bounds of the triangular lattice configurations, the spatial separation evaluates to approximately 10 carbon bond lengths from substitution point to substitution point. The thermodynamic survival of these specific bridges into the mid-Proterozoic rock record formally establishes the inter-cluster separations measured in modern Ruthenium-ion catalyzed oxidation (RICO) and advanced NMR experiments, preserving the continuous-forbidden spatial logic of the original metamaterial.

10 Conclusion

The macromolecular aromatic networks preserved in pre-Cambrian shale kerogens exhibit cluster sizes, bridge chemistries, dimensional scales and porous-matrix organization consistent with the abiotic-loom architecture of the Chrysene Formalism. The same networks supply a coherent geometric setting for metal and phosphorus integration, including rearrangement pathways that begin from the native C_{2h} symmetry of tetrasubstituted chrysene and proceed toward quasi-D_{4h} macrocycles compatible with geo-porphyrins of the heme and chlorophyll series.

While isomer-specific regiochemistry, individual ghost-pocket geometries and direct atomistic proof of the chrysene-to-porphyrin rearrangement remain beyond present analytical resolution, the existing experimental record already provides positive consistency tests at the level of network architecture and characteristic length scales.

Kerogen therefore offers a direct empirical pathway for the progressive confirmation of the Chrysene Formalism in the pre-Cambrian sedimentary record, complementary to the free-biomarker archive and continuous with the transition from environmental loom to endogenous cellular matrix.

A Literature Review: Pre-Cambrian Kerogen Networks and Related Observables

The empirical foundation of the present work rests on a substantial body of analytical studies of pre-Cambrian sedimentary organic matter. The following summary records the principal observational constraints that any geometric model of macromolecular aromatic networks must respect.

A.1 Aromatic Structure and Cluster Size

Solid-state ^{13}C NMR spectroscopy has repeatedly shown that pre-Cambrian and early Paleozoic kerogens are dominated by aromatic carbon, with average cluster sizes lying in the small fused-ring regime [MLS+07, H+18, MFL+10]. Typical estimates range from one to a few condensed rings in less mature material, increasing only modestly with thermal stress. These observations are consistent with the dominance of small aromatic clusters rather than extensive graphitic sheets.

Catalytic hydropyrolysis (HyPy) releases covalently bound polycyclic aromatic hydrocarbons from Archean and Proterozoic kerogens [BLS+03, LSG+08]. The product distributions are characterized by parent and lightly alkylated PAHs (phenanthrene, pyrene and higher homologues), confirming that aromatic units are embedded in a macromolecular network rather than existing solely as free bitumen.

Raman spectroscopy supplies independent constraints on the degree of aromatic condensation and short-range order [MLS+07]. The resulting parameters (I_D/I_G, peak positions) track maturity and are compatible with limited stacking of small aromatic domains.

A.2 Bridging Chemistry and Network Architecture

NMR spectra of pre-Cambrian kerogens routinely display aliphatic and oxygen-substituted carbon resonances in addition to the aromatic signal [MFL+10, H+18]. These resonances are interpreted as bridges linking aromatic clusters, forming a covalently cross-linked macromolecular matrix. Hydropyrolysis and solvent-extraction comparisons further demonstrate that a substantial fraction of the aromatic inventory is covalently bound [BLS+03, LSG+08].

X-ray diffraction and wide-angle scattering studies of kerogens and related carbonaceous materials yield average interlayer spacings (d_{002}) typically in the range 3.4–3.7 Å and lateral crystallite sizes of only a few to tens of ångströms [LJZ+22]. Such values are consistent with short-range π-stacking of small aromatic units rather than long-range graphitic order.

A.3 Metals, Porphyrins and Phosphorus

Nickel and vanadyl petroporphyrins are well-documented constituents of sedimentary organic matter and petroleum [Tre36, DAPE75]. Intact geoporphyrins have been recovered from 1.1-billion-year-old black shales, extending the porphyrin record deep into the Proterozoic [GMO+18]. Bulk analyses likewise show enrichment of Ni, V and Fe in many pre-Cambrian kerogens.

Phosphorus is present in measurable quantities in organic-rich pre-Cambrian sedimentary sequences, although spatially resolved associations between phosphorus and metal centres within the kerogen matrix remain sparsely documented.

A.4 Porosity and Dimensional Scales

Small-angle X-ray and neutron scattering studies of isolated kerogens reveal pore-size distributions that commonly include a population of nanometre-scale voids [LJZ+22]. These data establish that the macromolecular network is porous on the scale of tens of ångströms, providing an experimental window onto inter-cluster separations and interstitial volume.

A.5 Summary of Empirical Boundary Conditions

Collectively the literature establishes that pre-Cambrian shale kerogens contain:

1. a macromolecular aromatic network dominated by small fused-ring clusters,
2. aliphatic and ether-type bridges linking those clusters,
3. short-range π-stacking with interlayer distances near 0.35–0.37 nm,
4. a nanoporous matrix whose characteristic void dimensions overlap the 5–15 Å window,
5. associated metals (especially Ni, V, Fe) and phosphorus, and
6. , in favourable cases, geoporphyrins of biological ancestry.

These observables constitute the experimental boundary conditions against which the geometric predictions of the Chrysene Formalism are tested in the main text.

B Relation to the Chrysene Formalism Corpus

The present work belongs to a continuing programme whose empirical and mathematical foundations have been set out in earlier publications.

The experimental starting point is the composition-of-matter discovery that nucleic-acid sequences integrated within a phospholipid enclosure can be generated directly from a substituted chrysene precursor [Sch25]. That result supplied the concrete molecular geometry whose abstraction yields the pure-mathematical structure known as the Chrysene Formalism.

The Formalism itself is developed in two complementary volumes. The first constructs the discrete non-commutative state space, its cohomological invariants and the associated operator algebras [Sch26b]. The second supplies the tensorial and algebraic-geometric framework that governs maximal-entropy survival under topological strain [Sch26d]. Together these works define the manifold $\mathcal{I}_C$ and the structure-preserving maps that relate it to physical realisations.

Subsequent articles in the *Annals* have applied the same geometry to successive layers of biological organisation. One examines the tetrasubstituted chrysene lattice as a programmable topological metamaterial capable of self-assembly and quantum-information encoding [Sch26c]. Another treats the dual-chrysene reactive volume as the source of the observed hopanoid–sterane asymmetry and of the transition from environmental to endogenous supply of membrane scaffolds [Sch26a]. A third presents the broader claim that a single encodable topological metamaterial accounts for the origin, the intelligence architecture and the evolutionary trajectory of life [Sch26e].

The present paper extends that programme into the geological record. It asks whether the macromolecular aromatic networks preserved in pre-Cambrian shale kerogens retain geometric signatures—cluster-size distribution, bridge-length spectrum, π-stacking distances, interstitial voids and metal-coordination motifs—that are the expected images under the realisation map $\Phi : \mathcal{I}_C \to \mathcal{L}$. By confronting the predictions of the Formalism with the existing analytical data on mid-Proterozoic and older kerogens, the work tests the consistency of the pure-mathematical construction with the longest available chemical archive of early life and thereby supplies an independent empirical constraint on the entire series.

References

[BLS+03] Jochen J. Brocks, Gordon D. Love, Colin E. Snape, Graham A. Logan, Roger E. Summons, and Roger Buick. Release of bound aromatic hydrocarbons from late Archean and Mesoproterozoic kerogens via hydropyrolysis. *Geochimica et Cosmochimica Acta*, 67(8):1521–1530, 2003.

[DAPE75] Borys M. Didyk, Yousif I. A. Alturki, Colin T. Pillinger, and Geoffrey Eglinton. Petroporphyrins as indicators of geothermal maturation. *Nature*, 256:563–565, 1975.

[GMO+18] N. Gueneli, A. M. McKenna, N. Ohkouchi, C. J. Boreham, J. Beghin, E. J. Javaux, and J. J. Brocks.

1.1-billion-year-old porphyrins establish a marine ecosystem dominated by bacterial primary producers. *Proceedings of the National Academy of Sciences*, 115:E6978–E6986, 2018.

[H+18] L. Huang et al. Molecular structure characterization of Cambrian kerogen by solid-state ^{13}C NMR and XPS. *Search and Discovery Article*, 2018. Adapted from oral presentation.

[LJZ+22] Kou-Qi Liu, Zhi-Jun Jin, Lian-Bo Zeng, Meng-Di Sun, Bo Liu, Ho Won Jang, Majid Safaei-Farouji, Mohammadreza Shokouhimehr, and Mehdi Ostadhassan. Microstructural analysis of organic matter in shale by SAXS and WAXS methods. *Petroleum Science*, 19:979–989, 2022.

[LSG+08] Gordon D. Love, Charlotte Stalvies, Emmanuelle Grosjean, Will Meredith, and Colin E. Snape. Analysis of molecular biomarkers covalently bound within Neoproterozoic sedimentary kerogen. *The Paleontological Society Papers*, 14:67–83, 2008.

[MFL+10] Jingdong Mao, Xiaowen Fang, Yeqing Lan, Arndt Schimmelmann, Maria Mastalerz, Li Xu, and Klaus Schmidt-Rohr. Chemical and nanometer-scale structure of kerogen and its change during thermal maturation investigated by advanced solid-state ^{13}C NMR spectroscopy. *Geochimica et Cosmochimica Acta*, 74:2110–2127, 2010.

[MLS+07] Craig P. Marshall, Gordon D. Love, Colin E. Snape, Andrew C. Hill, Abigail C. Allwood, Malcolm R. Walter, Martin J. Van Kranendonk, Stephen A. Bowden, Sean P. Sylva, and Roger E. Summons. Structural characterization of kerogen in 3.4 Ga Archaean cherts from the Pilbara Craton, Western Australia. *Precambrian Research*, 155:1–23, 2007.

[Sch25] Charles D. Schaper. Encoded design integrated synthesis of nucleic acids, and phospholipids, and related pharmaceutical products, 2025. Patent US 12,195,423.

[Sch26a] Charles D. Schaper. Differential catalyst geometries of the dual-chrysene metamaterial: Hopanoid–sterane asymmetry and the transition from environmental to endogenous supply annals of the chrysene formalism. *Annals of the Chrysene Formalism*, 1:196–208, 2026.

[Sch26b] Charles D. Schaper. *Foundations of the Chrysene Formalism: Cohomological Invariants, Operator Algebras, and the Discrete Noncommutative State Space*. Schaper Systems Press, San Francisco, CA, 2026. ISBN: 979-8-950371-08-0.

[Sch26c] Charles D. Schaper. Programmable topological metamaterials: Self-assembly and quantum information encoding in the tetrasubstituted chrysene lattice. *Annals of the Chrysene Formalism*, 1:169–177, 2026.

[Sch26d] Charles D. Schaper. *Tensorial Framework of the Chrysene Formalism - Universal Algebraic Geometry and Maximal-Entropy Survival*. Schaper Systems Press, San Francisco, CA, 2026. ISBN: 979-8-950371-03-5.

[Sch26e] Charles D. Schaper. The universal blueprint: One encodable topological metamaterial to explain the origin, intelligence, and evolution of life. *Annals of the Chrysene Formalism*, 1:178–195, 2026.

[Tre36] Alfred Treibs. Chlorophyll- und häminderivate in organischen mineralstoffen. *Angewandte Chemie*, 49:682–686, 1936.